

Cosmic Rays below $Z = 30$ in a diffusion model: new constraints on propagation parameters.

D. Maurin

*Laboratoire de Physique Théorique LAPTH, Annecy-le-Vieux, 74941, France
Université de Savoie, Chambéry, 73011, France*

maurin@lapp.in2p3.fr

F. Donato¹

Laboratoire de Physique Théorique LAPTH, Annecy-le-Vieux, 74941, France

donato@lapp.in2p3.fr

and

R. Taillet and P. Salati

*Laboratoire de Physique Théorique LAPTH, Annecy-le-Vieux, 74941, France
Université de Savoie, Chambéry, 73011, France.*

taillet@lapp.in2p3.fr, salati@lapp.in2p3.fr

ABSTRACT

Cosmic ray nuclei fluxes are expected to be measured with high precision in the near future. For instance, high quality data on the antiproton component could give important clues about the nature of the astronomical dark matter. A very good understanding of the different aspects of cosmic ray propagation is therefore necessary. In this paper, we use cosmic ray nuclei data to give constraints on the diffusion parameters. Propagation is studied with semi-analytical solutions of a diffusion model, and we give new analytical solutions for radioactively produced species. Our model includes convection and reacceleration as well as the standard energy losses. We perform a χ^2 analysis over B/C data for a large number of configurations obtained by varying the relevant parameters of the diffusion model. A very good agreement with B/C data arises for a number of configurations, all of which are compatible with sub-Fe/Fe data. Different source spectra $Q(E)$ and diffusion coefficients $K(E)$ have been tried, but for both parameters only one form gives a good fit. Another important result is that models without convection or without reacceleration are excluded. We find that the various parameters, *i.e.* the diffusion coefficient normalisation K_0 and spectral index δ , the halo thickness L , the Alfvén velocity V_a , and the convection velocity V_c are strongly correlated. We obtain limits on the spectral index δ of the diffusion coefficient, and in particular we exclude a Kolmogorov spectrum ($\delta = 1/3$).

¹INFN post-doctoral Fellow

1. Introduction

Understanding the composition and spectral features of cosmic rays has always been an astrophysical challenge. On one hand, the observational data have long been scarce and suffered from large uncertainties. On the other hand, the theoretical predictions to which these data should be compared to have also suffered from several drawbacks. Composition and spectra arise from the nuclear interaction of an initial distribution of energetic particles with interstellar matter (*spallations*) and their electromagnetic interactions with galactic magnetic fields (*acceleration* and *diffusive reacceleration*). First, the nuclear cross sections to be used were not very well known until recently. Second, our knowledge of the galactic magnetic field is far from complete. Cosmic rays are sensitive to its scale inhomogeneities (*diffusion*) which are not well observed. They are also sensitive to the presence of plasma shock-waves (acceleration in localized sources and diffusive reacceleration). Third, composition and spectra are altered as the cosmic rays enter the solar magnetic field, so that some more modelling has to be done in order to infer interstellar spectra from observations.

However, despite these sources of uncertainty, some gross features of the cosmic ray properties are well established. First, the study of secondary-to-primary ratio shows that a cosmic ray has crossed an average of about $x = 9 \text{ g cm}^{-2}$ of interstellar matter between its acceleration and its detection. Second, the isotopic ratio of radioactive species shows that it took about $\tau = 20 \text{ Myr}$ between the same events. As cosmic rays have a velocity close to c , we can infer the average density of the medium to be $n = x/(\tau c m_H) \approx 0.3 \text{ cm}^{-3}$. As the disk density is about 1 cm^{-3} , the cosmic rays must spend a fraction of time in an empty region, called the *diffusion halo*. Cosmic rays are produced and destroyed in the galactic disk, they diffuse in a larger zone whose characteristics are not well known, and eventually they can escape from this zone. To have a good modelling of cosmic ray propagation, we should know the geometry and size of the diffusion zone, the characteristics of the galactic magnetic field, and the sources.

In this paper, we use the existing data on nuclei, gathered by balloon-borne and space experiments during the last thirty years, to put constraints on the parameters describing the propagation of cosmic ray nuclei. One consequence is that many of the large uncertainties affecting the calculation of the antiproton flux could be strongly reduced (F. Donato & al., in preparation (12)). This is of utmost relevance for the study of exotic sources of antiprotons and antideuterons.

2. The diffusion model

It has been recognized for a long time that the relevant physical propagation model to be used is the diffusion model (Berezinskii & al. 1990; Ginzburg & Syrovatskii 1964), though the so-called leaky box model has been widely preferred for decades because of its simplicity.

The steady-state differential density $N^j(E, \vec{r})$ of the nucleus j as a function of energy E

and position \vec{r} in the Galaxy, is given by (see for instance Berezhinskii & al. 1990)

$$\nabla \cdot (K^j \nabla N^j - V_c N^j) - \frac{\partial}{\partial E} \left(\frac{\nabla \cdot V_c}{3} E_k \left(\frac{2m + E_k}{m + E_k} \right) N^j \right) + \frac{\partial}{\partial E} (b^j N^j) - \frac{1}{2} \frac{\partial^2}{\partial E^2} (d^j N^j) + \tilde{\Gamma}^j N^j = q^j + \sum_{m_k > m_j} \tilde{\Gamma}^{kj} N^k$$

The first terms represent diffusion (K^j is the diffusion coefficient) and convection (V_c is the convection velocity). The divergence of this velocity, expressed in the next term gives rise to an energy loss term connected with the adiabatic expansion of cosmic rays. Further, we have to take into account ionization and coulombian losses (the energy loss coefficients are specified below), plus a reacceleration term in first order derivative (all included in b^j) and finally a second order derivative in E for the associated second order term in reacceleration (d^j is the energy diffusion coefficient). These stand for the continuous losses. The last term of the l.h.s. takes care of the disappearance of the nucleus j ($\tilde{\Gamma}^j$ for short) due to its collisions with interstellar matter (ISM). In the r.h.s., the source term q^j takes into account the primary production and acceleration of nuclei described by an injection spectrum (for the sake of clarity, we have not written down the terms describing the contribution of radioactive species). Finally, the last term is for the secondary j sources, namely spallation contribution² $\tilde{\Gamma}^{kj}$ from all other heavier nuclei. We use here the notation E for total energy and E_k for kinetic energy.

One needs to solve a complete triangular-like set of coupled equations since only heaviest nuclei contribute to a given nucleus. Quantities in this equation are functions of spatial coordinates (not time, steady-state being assumed) and of energy. Unless stated otherwise, the word *energy* will stand for *kinetic energy per nucleon* (T), since this is the appropriate parameter to be used, as it is conserved in spallation reactions (see footnote 2).

The other very popular model is the leaky box, in which all the quantities are spatially averaged (so that convection has no meaning), and the diffusion term is then replaced by an escape term

$$-\nabla \cdot (K^j \nabla N^j) \longleftrightarrow \bar{N}^j / \tau_{esc}$$

which has the meaning of a residence time τ_{esc} (Myr) in the confinement volume. Note that in this case, the mean time $\langle \tau \rangle$ spent in the box and the mean column density $\langle x \rangle$ (in units of g cm^{-2}) of crossed matter are treated on the same footing since the model is homogeneous. This is not true for multi-zone models and especially for the diffusion model where cosmic rays spend most of their time in the diffusion halo which has a zero matter density. It may seem very surprising that this simplified model is able to reproduce many observations on stable nuclei. Actually, it can be shown that leaky box models are often equivalent to diffusion models, as far as stable species are concerned (for a generic discussion on the “leakage–lifetime” approximation in cosmic ray diffusion, see Jones 70). This is not obvious from the equations, but it can be seen more readily if we solve them in a formalism called the weighted slab technique. Basically,

²We use here the so-called straight-ahead approximation which implies the conservation of kinetic energy per nucleon during a spallation process

$$\int_0^\infty n_H v' N^k(T') \sigma^{kj}(T, T') dT' = \int_0^\infty n_H v' N^k(T') \sigma^{kj}(T) \delta(T - T') dT' = n_H v N^k(T) \sigma^{kj}(T) \quad (2)$$

it consists in writing a general solution under the form (see for example Berezhinskii et al. 1990; Ginzburg & Syrovatskii 1964)

$$N^j(\mathbf{r}) = \int_0^\infty \tilde{N}^j(x)G(\mathbf{r}, x)dx \quad (3)$$

Thus, (1) decouples into two independent equations. The first one involves $G(\mathbf{r}, x)$. It depends only on the geometry of the problem and on the chosen diffusion scheme (or the leaky box parameters), but not on the particular species j . The other one involves $\tilde{N}^j(x)$ and contains the nuclear physics aspects of the propagation. Different models (diffusion or leaky box) correspond to different $G(\mathbf{r}, x)$, but the equations on $\tilde{N}^j(x)$ are the same. G is the path length distribution and is interpreted as the distribution of probability that a nucleus j goes through a column density x before reaching Earth. The global solution is then obtained by a convolution of the surviving quantity $\tilde{N}^j(x)$ under nuclear processes after x g cm⁻², with the weighted probability associated.

In a leaky box model, it can be shown that the normalized path length distribution function is given by

$$G(x) = \frac{1}{\lambda_{\text{esc}}} \exp\left(\frac{-x}{\lambda_{\text{esc}}}\right) \quad (4)$$

where the average quantity of matter crossed by a cosmic ray is given by

$$\langle x \rangle = \int_0^\infty xG(x) dx = \lambda_{\text{esc}} \quad (5)$$

In the diffusion model, it has been shown (Owens 1976) that for a wide class of geometries, the function G is given by an infinite series of exponentials involving the diffusion coefficient. Moreover, the physical parameters are such that for sufficiently large grammage x , only the first exponential contributes so that we recover a leaky box model (Jones 1970; Ginzburg, Khazan & Ptuskin 1980; Schlickeiser & Lerche 1985; Lerche & Schlickeiser 1985). For the model used in this paper, it can be shown that $\lambda_{\text{esc}} = \bar{m}nvhL/K$ in the limit $L \ll R$. However, this is no longer true for lower x , and then the leaky box model fails. This may explain, in conjunction with poorly known cross sections for heavy nuclei, why for many years cosmic ray physicists had to use modifications (Lezniak & Webber 1979; Garcia-Munoz & al. 1987; Webber & al. 1998b) of the leaky box path length distribution at small grammage to reconcile observations of B/C with those of sub-Fe/Fe. Even worst, this approximate equivalence between leaky box and diffusion model breaks down for radioactive species (Prishchep & Ptuskin 1975).

This motivates us to choose the diffusion model and solve the corresponding equation (1). From a more general point of view, note also that the weighted slab technique mentioned above should be used carefully. Actually, it was recently realized (Ptuskin, Jones & Ormes 1996) that pre-1996 estimations of cosmic ray parameters with this technique were not exact. First, at fixed energy per nucleon, the rigidity and therefore the propagation features depend on the nuclear species, whatever the energy. This prevents the above-mentioned decoupling. Second, energy losses that strongly depend on A and Z also take place at low energy. Ptuskin et al. 1996 presented a modification of this formalism which is correct in both the highly and non-relativistic regimes. These fundamental findings were confirmed by a more complete numerical treatment (Stephens & Streitmatter 1998) and give rise to differences of as much as 20%.

For the nuclear part, we adopted the direct approach of the shower technique. This means that the flux is first evaluated for the heavier primary cosmic ray, for which the diffusion equation is simple and does not couple to any other species. Then, the flux of the next nucleus is computed, with a spallation term depending only on the heavier nucleus, whose flux is known from the previous step. This procedure is repeated for all the nuclei down to the lightest one. We started at $Z = 30$, the heavier non negligible primary found in cosmic radiation (Binns & al. 1989), since $(Z > 30) \leq 10^{-3}$ Fe. For all light nuclei, we checked that it is sufficient to start from $Z = 16$ (S). For the detail of solutions, the reader is referred to Appendix A. The next section is devoted to the inputs of the model.

3. The parameters of the model

3.1. Geometry of the Galaxy

The geometry of the problem used here is a classical cylindrical box (see for example Webber et al. 1992) whose radial extension is R , with a disk of thickness $2h$ and a halo of half-height L . Only L is not fixed (see §5) and $R = 20$ kpc, $h = 100$ pc. Sources and interactions with matter are confined to the thin disk and diffusion which occurs throughout disc and halo with the same strength is independent of space coordinates. The solar system is located in the galactic disc ($z = 0$) and at a centrogalactic distance $R_{\odot} = 8$ kpc (Stanek & Garnavich 1998; Alves 2000).

3.2. Cross sections

Cross sections play a crucial role in propagating the cosmic rays throughout the Galaxy. We have to distinguish between the total inelastic cross section and the spallation cross section.

3.2.1. Total inelastic cross section

The total inelastic cross section, which is actually a reaction cross section, is defined by

$$\sigma_{inel}^{tot} = \sigma^{tot} - \sigma_{elastic}^{tot} \quad (6)$$

Various empirical modifications of the original (Bradt & Peters 1950) geometrical approach have been used to parameterize this total cross section. Letaw, Silberberg & Tsao (1983) and Silberberg & Tsao (1990) produced the basic energy dependent equations further refined in Sihver & al. (1993) and in Wellish & Axen (1996). Recently Tripathi, Cucinotta & Wilson (1997a, 1997b, 1999) proposed a universal parameterization which is valid for all nucleus–nucleus reactions, including neutron induced reaction. All of these approaches have been compared in Silberberg, Tsao & Barghouty (1998), where the preference were given to Tripathi et al. (1997a, 1997b, 1999). For this reason, we adopted the latter parameterization throughout this study. The precision can be estimated to be about 5%.

3.2.2. Spallation cross section

The fragmentation cross sections are somewhat more complicated. Basically, we can separate three distinct approaches : (i) microscopical description (Bondorf & al. 1995; Ramsey & al. 1998) (ii) semi-empirical formulae (Silberberg et al. 1998; Tsao, Silberberg & Barghouty, 1998; Tsao et al. 1999) and (iii) empirical formulae (Webber, Kish & Schrier 1990d). The first one takes into account the fundamental nuclear physics but is very computer time consuming and has not reached a precision as good as the two other approaches. The second method takes into account more phenomenological inputs, and is better designed for the unmeasured fragmentation cross sections which correspond mainly to the ultra heavy ($Z \geq 30$) nuclei. The third one breaks down in this region, but can be used for $3 \leq Z \leq 30$ because it is adapted to fit measurements. Consequently, we used the code of Webber et al. (1990d) available on the web ³ updated with new parameters (table V of Webber & al. 1998a). This parameterization takes advantage of the fact that about 98% of all the reaction involved in cosmic ray propagation have now at least one point of energy measured. This set of formulae gives a precision of about 10% but can not be further refined (Webber et al. 1998a). The code is extended for spallation on He with the parameterization given in Ferrando et al. (1988)⁴.

To go further than this treatment, one should keep in mind the following points. First, the process of single or double nucleon removal is an important channel for the production of numerous nuclei. It has been parameterized in detail in Norbury & Townsend (1993) and in Norbury & Mueller (1994), although in the following we will consider Webber’s approach sufficient for our purpose. Second, most of the parameterizations make use of the straight-ahead approximation (see footnote 2). Tsao & al. (1995) relaxed this condition and find a 5% effect around the 1 GeV peak of B/C (note that this effect is negligible for primary to primary and secondary to secondary ratios). Finally, it was found that all the measurements are not always consistent and systematic effects are likely to be present (Taddeucci & al. 1997; Vonach & al. 1997; Zeitlin & al. 1997; Flesh & al. 1999; Korejwo & al. 1999).

To summarize, we consider that Webber’s code is very well suited for modelling spallation cross sections, thanks to the many experiments developed these last years (Webber, Kish & Schrier 1990a, 1990b, 1990c; Webber et al. 1998b, 1998c; Chen et al. 1997). The overall precision can be roughly estimated to be better than 10% on H, and better than 20% on He.

3.3. Nuclear parameters

Apart from the stable species, we can distinguish two categories of nuclei to be propagated, depending on whether they live long enough to be observed or they decay quickly into other nuclei.

³http://spdsch.phys.lsu.edu/SPDSCH_Pages/Software_Pages/Cross_Section_Calcs/CrossSectionCalcs.html

⁴The parameterization given in this paper should be modified at low energy and for large ΔZ (P. Ferrando 2001, private communication).

3.3.1. Ghost nuclei

Ghost nuclei are defined as those having a half–lifetime larger than ~ 1 ms (so that they are detected in cross section measurements) and less than few hundred years (so that we can consider that disintegration is fast on a propagation timescale). Several reaction channels may yield a given nucleus. This means that for this nucleus, we have to add to the direct production the contributions of all the short lived parent nuclei

$$\sigma_{k \rightarrow j}^{effective} = \sigma_{kj} + \sum_{\text{nuclei } X}^{ghost} \sigma_{k \rightarrow X} \mathcal{B}r(X \rightarrow j) \quad (7)$$

where $\mathcal{B}r(X \rightarrow j)$ is the branching ratio of the corresponding channel⁵. A table of all the disintegration chains can be found in Letaw & al. 1984. To see the effect of the recent discovery of new intermediate short–lived nuclei and of the changes in branching ratio, we reconstructed from a recent compilation of nuclear properties (Audi et al. 1997) all the ghost nuclei and compared them with the Letaw table. We found that the net effect is negligible. This is because the discovered radioelements are very far from the valley of stability and their production is suppressed (as it can be observed experimentally). Such reaction chains should accordingly be taken as a fixed input for the future.

3.3.2. Radioactive nuclei

Radioactive nuclei can be separated into three groups : unstable under β decay, unstable under electronic capture and unstable under both reactions. All the physical effects related to these nuclei will be analysed in detail in a separate paper (F. Donato & al., in preparation (13)).

3.4. Diffusion coefficient

Physically, diffusion arises because charged particles interact with the galactic magnetic field inhomogeneities. This is an energy–dependent process because higher energy particles are sensitive to larger spatial scales. As a result, the diffusion coefficient is related to the power spectrum of these inhomogeneities, which is poorly known. Several analytical forms of this energy dependence have been assumed in the literature. In particular, leaky box models give a purely phenomenological form

$$\begin{cases} \lambda_{\text{esc}} = \lambda_0 \beta & \text{if } \mathcal{R} < \mathcal{R}_c \text{ in GV} \\ \lambda_{\text{esc}} = \lambda_0 \beta (\mathcal{R}/\mathcal{R}_c)^{-\delta} & \text{if } \mathcal{R} > \mathcal{R}_c \text{ in GV} \end{cases}$$

⁵To give an example, such a reaction reads for ${}^9_4\text{Be}$

$$\sigma_{k \rightarrow {}^9_4\text{Be}}^{effective} = \sigma_{i \rightarrow {}^9_4\text{Be}} + 49.2\% \sigma_{k \rightarrow {}^9_3\text{Li}} + 4.1\% \sigma_{k \rightarrow {}^{11}_3\text{Li}} \quad (8)$$

where $\mathcal{R} = p/Z$ stands for the particle rigidity. A more fundamental origin may be found for the previous expression, as one can show in a one-dimensional diffusion model with convection (Jones & al. 2001). All the effects that led to that phenomenological form are explicitly taken into account in our treatment and we may therefore consider a more natural form for $K(E)$, inferred from magnetohydrodynamics considerations (Ptuskin et al. 1997):

$$K(E) = K_0 \beta \times \mathcal{R}^\delta \quad (9)$$

where the normalisation K_0 is expressed in $\text{kpc}^2 \text{Myr}^{-1}$. Nevertheless, we have also tested leaky box inspired forms, but these never give good fits to the data (see next section).

3.5. Sources

A charged particle is called a cosmic ray when it has been accelerated to an energy greater than 100 MeV/n as far as our study is concerned. Several physical processes may be responsible for this energy gain; they all involve an interaction of the particle with a plasma shockwave front. This is responsible for the power-law energy dependence (see below). The term *source* refers to the place where the charged particles have been promoted to cosmic rays. We present here the various hypotheses about their spatial and spectral distributions and their compositions.

3.5.1. Spatial distribution

First, as explained above, we assumed that the Galaxy has a cylindrical symmetry and that the sources are located in the galactic disc. So we only have to specify a radial distribution. We have used the Case & Bhattacharya (1996, 1998) distributions, but the results presented below are not sensitive to this particular choice.

3.5.2. Spectral distribution

The source spectral distributions can be split in two terms

$$q^j(E) = q_0^j Q^j(E) \quad (10)$$

where q_0^j represent the composition and $Q^j(E)$ the energy dependence. Several spectra have been used in the past (Engelmann & al. 1985),

$$\begin{aligned} Q^j(E) &\propto p^{-\alpha_j} \\ Q^j(E) &\propto \beta E_{kin}^{-\alpha_j} \\ Q^j(E) &\propto E_{tot}^{-\alpha_j} \end{aligned} \quad (11)$$

where p is the momentum and where the spectral index α_j may depend on the species j considered. These forms are equivalent at high energies but we focused on the first one only (equivalent to a power-law in rigidity) as the others do not yield good fits to the data. The sum $\delta + \alpha_j$

gives the overall power-law index of each species at high energy (≈ 1 TeV/ n): this is because the measured flux at these energy is proportional to $Q^j(E)/K(E) \propto \mathcal{R}^{\delta+\alpha_j}$. In other words, at sufficiently high energy, energetic redistribution and spallation reactions do not affect propagation. Consequently, measured spectral indexes enter as a fixed input, and we took them in Wiebel–Sooth, Biermann & Meyer (1998). For consistency, we required that whatever δ , the parameters α_j are adjusted so as to reproduce the above-mentioned values. This ensures that the spectra we compute agree with data at high energy.

3.5.3. Composition

The composition q_0^j is usually inferred from a comparison between leaky box calculations and data. Alternatively, a more fundamental approach can be used. It may be taken either as the solar system composition convoluted with the FIP (First Ionisation Potential), or convoluted with the volatility. As pointed out in Webber (1997), the two alternatives are not so different. In this work, the isotopic composition of each element was taken from Anders & Grevesse (1989) and Grevesse & Sauval (1998), and the q_0 dependence of the FIP has been taken from Binns et al. (1989). Then the primary cosmic ray elemental composition has been adjusted to fit the HEAO-3 data at 10.6 GeV/ n , while keeping constant the relative isotopic abundances.

3.6. Galactic wind, energy loss, reacceleration

Once we have chosen a generic model, we have to include effects which affect the spectra at low energies. A first step is the inclusion of energetic losses. Then a most complete treatment must take into account reacceleration and convection.

3.6.1. Energy losses

There are two types of energy losses which are relevant for nuclei: ionization losses in the ISM neutral matter (90% H and 10% He), and Coulomb energy losses in a completely ionized plasma, dominated by scattering off the thermal electrons. We will use $\langle n_e \rangle \sim 0.033$ cm $^{-3}$, and $T_e \sim 10^4$ K (Nordgren 1992). Complete formulae for these two effects are compiled, for example, in Strong & Moskalenko (1998) or in Mannheim & Schlickeiser (1994). There is also a third type of loss related to the existence of a galactic wind. We recall that in equation (1), there is a term proportional to $\nabla \cdot V_c$. As we choose a constant wind velocity in the z direction (see farther), we could conclude at a first glance that this term vanishes. Actually, this is the case everywhere in the Galaxy except at $z = 0$ where a discontinuity occurs, due to the opposite sign of the wind velocity above and below the galactic plane. One gets a term that can be expressed in the same form as ionization and coulombian losses with an effective term

$$\left\langle \frac{dE}{dt} \right\rangle_{Adiab} = -E_k \left(\frac{2m + E_k}{m + E_k} \right) \frac{V_c}{3h} \quad (12)$$

E_k stands for the total kinetic energy and it should not be confused with the kinetic energy per nucleus frequently used in this paper. Finally, because of these effects the propagation equation must be solved numerically.

3.6.2. Reacceleration

As the fractional energy changes in a single collision are small, we can treat Fermi acceleration (Fermi 1949; 1954) using the Fokker–Planck formalism (Blandford & Eichler 1987). In one dimension

$$\frac{\partial f}{\partial t} + v \frac{\partial f}{\partial x} = \frac{\partial}{\partial p} \left[- \left\langle \frac{\Delta p}{\Delta t} \right\rangle f + \frac{1}{2} \frac{\partial}{\partial p} \left(\left\langle \frac{(\Delta p)^2}{\Delta t} \right\rangle f \right) \right] \quad (13)$$

where $\langle \Delta p / \Delta t \rangle$ and $\langle (\Delta p)^2 / \Delta t \rangle$ are expressed in terms of the probability for changing the momentum p to $p + \Delta p$ during time Δt . A simplification occurs when the recoil of the scatterer can be ignored. In general, the principle of detailed balance ensures that the probability for a gain is equal to that for a loss. This implies

$$\left\langle \frac{\Delta p}{\Delta t} \right\rangle = \frac{1}{2} \frac{\partial}{\partial p} \left\langle \frac{(\Delta p)^2}{\Delta t} \right\rangle \quad (14)$$

which reduces the equation into

$$\frac{\partial f}{\partial t} + v \frac{\partial f}{\partial x} = \frac{\partial}{\partial p} K_{pp} \frac{\partial}{\partial p} (f) \quad (15)$$

where

$$K_{pp} \equiv \frac{1}{2} \left\langle \frac{(\Delta p)^2}{\Delta t} \right\rangle \quad (16)$$

From another point of view, we can start with a collisionless Boltzmann equation and expand it up to second order in perturbed quantities (magnetic irregularities). It gives the full diffusion equation in quasi-linear theory (Schlickeiser 1986; Kulsrud & Pearce 1969). Assuming a constant flow of magnetic irregularities (corresponding to a constant galactic wind) in the z direction, we find

$$\frac{\partial f}{\partial t} = -V_c \nabla f + \nabla (K \nabla f) + \frac{1}{p^2} \frac{\partial}{\partial p} \left[K_{pp} p^2 \frac{\partial f}{\partial p} \right] + Q(r, p, t) \quad (17)$$

which is the propagation equation we used in Appendix A (up to several nuclear terms, cf eq. (A1)). In this theory, the momentum diffusion coefficient K_{pp} is naturally connected to the space diffusion coefficient K by the relation

$$K_{pp} = \frac{V_a^2}{9K} p^2 \quad (18)$$

where V_a is the Alfvén speed of the scattering centers.

We emphasize that expressions (15) and (17) are just simplifications of the full Fokker–Planck equations. As pointed out by Ostrowski & Siemieniec-Oziębło (1997), if this simplification is natural in the kinetic description of a gas of scattering particles, this is no longer the case

for particles scattered off external ‘heavy’ scattering centers. Nevertheless, this approximation which arises in a number of astrophysical cases is sufficient for our purpose. We thus have to treat a simple energy diffusion coefficient, which we evaluated in the no-recoil hard sphere scattering centers approximation as

$$K_{EE} \equiv \frac{1}{2} \left\langle \frac{(\Delta E)^2}{\Delta t} \right\rangle = \frac{2}{3} V_a^2 \frac{\sigma_K n_K}{c} E^2 \beta^3 \quad (19)$$

where $\sigma_K n_K$ describes the rate of collisions with scatterers which is related to the mean free path by $\lambda_K = 1/\sigma_K n_K$. As $K(E) = (1/3)\lambda_K v$, the previous relation gives the final coefficient to be used in our calculation

$$K_{EE} = \frac{2}{9} V_a^2 \frac{E^2 \beta^4}{K(E)} \quad (20)$$

Our approach is basically similar to that of Heinbach & Simon (1995). The meaning of the Alfvénic speed derived in their analysis is not very clear, since the numerical factor in front of expression (20) may vary according to the hypotheses made for the scattering process. The assumption that reacceleration occurs only in the thin disc is supported by recent complete magnetohydrodynamics simulations (Ptuskin et al. 1997) describing the evolution of the hot gas, cosmic rays and magnetic field.

3.6.3. Integration into equation

We define

$$b_{loss}^j(E) = \left\langle \frac{dE}{dt} \right\rangle_{Ion} + \left\langle \frac{dE}{dt} \right\rangle_{Coul} + \left\langle \frac{dE}{dt} \right\rangle_{Adiab} \quad (21)$$

and with $K_{EE}^j(E)$ given by (20), one obtains (see Appendix)

$$A_i^j N_i^j(0) = \bar{Q}^j - 2h \frac{\partial}{\partial E} \left\{ b_{loss}^j(E) N_i^j(0) - K_{EE}^j(E) \frac{\partial}{\partial E} N_i^j(0) \right\} \quad (22)$$

This is a second order equation which is solved for each order i of the Bessel decomposition. A_i^j is given by (A10) and \bar{Q}^j (A5) is a generic source term (see Appendix A for details). Relation (22) has been developed on our energy array so as to be transformed into a matrix equation that is directly inverted. Two boundary conditions need to be implemented. The effects of energy losses and diffusive reacceleration have been assumed to be negligible at the high energy tip (100 GeV/n) of the spectrum. We have furthermore imposed a vanishing curvature ($\partial^2 N_i^j / \partial E^2 = 0$) at the lowest energy point.

3.6.4. Galactic wind

It has been recognized for a long time that a thin disc configuration would be disrupted by cosmic ray pressure (Parker 1965, 1966; Ko, Dougherty & McKenzie 1991). It can be stabilized by the presence of a halo, but further considerations imply that this halo would not be static either (presence of a convective wind). Consequences of a wind has been firstly investigated

by Ipavitch (1975) and since then it has been observed in other galaxies (Lerche & Schlickeiser 1982a, 1982b; Reich & Reich 1988; Werner 1988). In our own, its effects on nuclei have been investigated in various models (Jones 1979; Kóta & Owens 1980; Freedman & al. 1980; Bloemen & al. 1993), and in this work we adopted a very simple and tractable form for V_c throughout the diffusive volume ($dV_c/dz = 0$), following Webber, Lee & Gupta (1992). A constant wind with free escape boundary is a reasonable approximation to a more sophisticated variable-wind model (see also conclusions from magnetohydrodynamics simulations (Ptuskin et al. 1997)).

3.6.5. Comparison with other works

Our semi-analytical two-dimensional model lies, in some sense, between the complete numerical resolution of Strong & Moskalenko (1998) and the recent study of Jones et al. (2001). As compared to the first one, we have a simplified description of the matter distribution, for which the full analysis of the parameter space does not require too much CPU time. The second approach can be considered as the limiting case for our two-dimension model when the radial extension is much larger than the halo size ($R \gg L$). Note that a similar analysis was performed by Letaw, Silberberg & Tsao (1993) in the framework of a leaky box model or Seo & Ptuskin (1994) in a one-dimensional diffusion model but their less systematic approach does not allow a full exploration of parameter space.

4. Data Analysis

For the aim of our analysis, we can consider different classes of flux ratios: primary-to-primary (*e.g.* C/O), secondary-to-primary (*e.g.* B/C or sub-Fe/Fe), secondary-to-secondary (*e.g.* Li/B or Be/B), ratio of isotopes either stable (*e.g.* $^{10}\text{B}/^{11}\text{B}$) or unstable (*e.g.* $^{10}\text{Be}/^9\text{Be}$). Each of these may be an indicator of some dominant physical phenomenon and be particularly sensitive to the corresponding diffusion parameters. The ratio of two primaries is practically insensitive to changes in all the parameters, since they have the same origin and undergo the same physical processes. So, it can be a very useful tool to fix their source abundances. We will return to this subject. Similar conclusions, even if less strong, may be drawn for the ratio of two isotopes of the same species, such as $^{10}\text{B}/^{11}\text{B}$. Indeed, at very low energy values this quantity is slightly affected by changes in the injection spectra, but the effect is too weak to constrain free parameters.

The most sensitive quantity is B/C, as B is purely secondary and its main progenitor C is primary. The shape of this ratio is seriously modified by changes in the diffusion coefficient, in the height of the diffusion halo, in the convective and alfvénic velocities. Moreover, it is also the quantity measured with the best accuracy, so that it is ideal to test models. Indeed, being the ratio of two nuclei having similar Z , it is less sensitive to systematic errors than single fluxes or other ratios of nuclei with more distant Z . For the same reasons, the sub-Fe/Fe may also be useful. Unfortunately, since existing data are still affected by sizeable experimental errors, we can only use them to cross-check the validity of B/C but not to further constrain

the parameters under scrutiny. Another particularly interesting quantity is the ratio $^{10}\text{Be}/^9\text{Be}$. Since ^{10}Be is a radioactive element, it is very sensitive to the processes which can occur in the halo. Therefore, we could use this ratio in particular to bracket the size of the halo (F. Donato & al., in preparation).

4.1. Solar modulation

We have estimated the effect of the solar wind on the energies and intensities of cosmic-rays following the prescriptions of the force field approximation (Perko 1987). The modification in the total interstellar energies of a nucleus with charge Z and atomic number A , corresponds to the shift $Z\phi$ (we set the electronic charge equal to unity):

$$E^{\text{TOA}}/A = E^{\text{IS}}/A - |Z|\phi/A. \quad (23)$$

Here E^{TOA} and E^{IS} correspond to the top-of-atmosphere (modulated) and interstellar total energy, respectively. The solar modulation parameter ϕ has the dimension of a rigidity (or an electric potential), and its value varies according the 11-years solar cycle, being greater for a period of maximal solar activity. Often people refer to the equivalent quantity $\Phi = |Z|\phi/A \simeq \frac{1}{2}\phi$. Once the momenta at the Earth p^{TOA} and at the boundaries of the heliosphere p^{IS} are determined, the interstellar flux of the considered nucleus is related to the TOA flux according to the simple rule:

$$\frac{\Phi^{\text{TOA}}(E^{\text{TOA}})}{\Phi^{\text{IS}}(E^{\text{IS}})} = \left\{ \frac{p^{\text{TOA}}}{p^{\text{IS}}} \right\}^2 \quad (24)$$

The determination of the modulation parameter Φ is totally phenomenological and suffers from some uncertainty. As explained in the following, we will deal with data taken around period of minimal solar activity, for which we fixed $\Phi = 250$ MV.

4.2. The dataset we used

In order to test our diffusion model we have widely employed the data taken by the experiment which was launched on board the NASA HEAO-3 satellite (Engelmann et al. 1990). The relative abundances of elements, with charge from 4 to 28 and for energy ranging from 0.6 to 35 GeV/n, have been measured with unprecedented accuracy. Data have been taken in 1979–80, around a solar minimal activity. For the case of B/C, HEAO-3 quoted errors are 2–3%. To perform the analysis, we also included data from balloons (Dwyer & Meyer 1987) and from the ISEE-3 experiment (Krombel & Wiedenbeck 1988), even if the relevant error bars are wider. The first one collected data in 1973–75 for energies spanning from around 1.7 to 7 GeV/n. The second experiment was operating during 1979–81 on board a spacecraft, in the energy range 100–200 MeV/n. In some of the figures presented below, we also plot – for purely illustrative goals – the data point from IMP-8 (Garcia-Munoz et al. 1987) and the VOYAGER experiments (Lukasiak, McDonald & Webber 1999) (we did not include Ulysse data point (DuVernois & al. 1996), since it corresponds to a period of maximal solar activity). They were not included in

the χ^2 analysis since they are the most sensitive to solar modulation. Nevertheless, we have checked that the best χ^2 values were not significantly modified when these points were added.

As regards the sub-Fe(Sc+V+Ti)/Fe ratio, we used data from HEAO-3 (Engelmann et al. 1990) and from balloons (Dwyer & Meyer 1987). In both cases the error bars, around 10%, are significantly larger than for B/C.

5. Results

We varied the relevant parameters K_0 , L , V_c , V_a , and δ of the diffusion model described above. The constraints are much simpler to express with the combinations L , K_0/L , V_c and $V_a/\sqrt{K_0}$ (this last expression appears naturally in $K_{EE}(E)$ describing reacceleration). As for the primaries, we have adjusted the source abundance for nitrogen which is not a pure secondary. We calculated the χ^2 over the 26 experimental points listed in 4.2, for each possible combination obtained varying the free parameters in the whole parameter space. In the following, we will focus on B/C and we cross-check the compatibility of the obtained parameters when applied to other fluxes.

5.1. Results of B/C and sub-Fe/Fe analysis for $\delta = 0.6$

In a first step, the power δ of rigidity in the expression for the diffusion coefficient (see Eq. (9)) has been fixed to 0.6. This will be the reference value for the bulk of our analysis. We only show models giving a χ^2 less than 40. The best models have $\chi^2 \approx 28$. Some of these configurations have a very small halo size in which case the condition $h \ll L$ is no longer valid. Thus we also required $L > 1$ kpc in the whole analysis.

The first result is that only the source spectrum $q^j(E) = q_0^j p^{-\alpha_j}$ gives a good fit to the data. It will be used all the way long. For each L and K_0/L , we vary $V_a/\sqrt{K_0}$ and V_c and the best χ^2 are shown in Fig. 1. All the good models are located in a narrow strip in the plane $L - K_0/L$, showing a strong correlation between these two parameters. However, there is still a degeneracy. It should be lifted with further specific analysis of radioactive nuclei (F. Donato & al., in preparation). Conversely, for each $V_a/\sqrt{K_0}$ and V_c we varied L and K_0/L and the best values for the χ^2 are depicted in Fig. 2. We see that they are gathered in a narrow range, namely: $8.5 \lesssim V_c \lesssim 12$ km sec⁻¹ and $410 \lesssim V_a/\sqrt{K_0} \lesssim 530$ km s⁻¹/ Mpc Myr^{-1/2}. We do not find any model having a good χ^2 without convection ($V_c = 0$) or without reacceleration ($V_a = 0$). We emphasize the fact that these four parameters are strongly correlated so that, when one of them is determined (for example L with radioactive nuclei), the allowed ranges for the others will be narrower than what could naively appear from the above two figures.

The observed sub-Fe/Fe flux ratio does not give very powerful constraints. Nevertheless, all the models which give a good fit to B/C data are consistent with sub-Fe/Fe data. Figures 3 and 4 illustrate these results with the particular choice $L = 9.5$ kpc, $K_0/L = 0.00345$ kpc Myr⁻¹, $V_c = 10.5$ km s⁻¹ and $V_a/\sqrt{K_0} = 470$ km s⁻¹/ Mpc Myr^{-1/2}, giving a reduced $\chi_r^2 \approx 1.3$. Note that all the configurations lying in the allowed ranges of Fig. 1 and 2 will provide very similar

curves.

Up to now we have dealt with flux ratios, which partially hide the spectral features of the fluxes themselves. So we have also checked that the above configurations were consistent with the oxygen flux as measured by HEAO–3. In Fig. 5 the oxygen flux has been calculated for the same configuration as in Fig. 3 and 4. We can notice that the agreement with HEAO–3 data is not so satisfactory. The parameter which mainly prevents us from obtaining a good fit is the source spectrum. We recall that we set the sum $\delta + \alpha_j$ to the power–low index as determined in Wiebel–Sooth et al. (1998). Indeed, this number for the oxygen species is equal to 2.68 as derived from HEAO–3 and many other measurements. If instead we fix $\delta + \alpha_{Oxygen}$ to be 2.8 (as in Swordy & al. (1993)), the fit improves (see Fig. 5).

5.2. Variation of the diffusion coefficient spectral index

We also tested different values for δ , and we find that correspondingly the diffusion parameters giving a good fit to B/C change. As an example, for a fixed value of the halo thickness $L = 3$ kpc, we find that δ is allowed to vary between 0.5 and 0.84. This is displayed in Fig. 6. In the whole parameter space, the range of δ extends from approximately 0.45 to 0.85, as one can see in Fig. 7. In particular the value $\delta = 0.33$ corresponding to a Kolmogorov–like turbulence spectrum is strongly disfavoured ($\chi^2 > 100$). For intermediate values of δ , good models are obtained for the full range in L (as in Fig. 1). For low values of δ , models with a small halo size L are excluded; in particular for $\delta < 0.45$, there is no good model with $L < 15$ kpc. Finally, for high values of δ , models with a large halo L are excluded, and for $\delta > 0.85$, there is no good model with $L > 1$ kpc. As can be seen in Fig. 7, each value of δ gives a different contour plot in the $K_0/L - L$ plane. It appears that they all can be superimposed to a single curve by a rescaling $K_0/L \rightarrow K_0/L \times f(\delta)$, where f is a function of δ only. For the contours displayed in Fig. 7, it takes the values $f(0.46) = 0.51$, $f(0.5) = 0.62$, $f(0.6) \equiv 1$, $f(0.7) = 1.54$ and $f(0.85) = 2.78$.

In the $V_a/\sqrt{K_0} - V_c$ plane, the values of V_c are shifted downward as δ is decreased but the allowed range of $V_a/\sqrt{K_0}$ does not significantly move. Nevertheless, the allowed values for V_c never reach 0, so that no–wind models can be excluded.

6. Discussion and conclusion

We obtain good quantitative constraints on the diffusion parameters from B/C data. In particular, there is a very strong correlation between L , K_0/L , V_c , $V_a/\sqrt{K_0}$ and δ . For $\delta = 0.6$, we find that $8.5 \text{ km s}^{-1} < V_c < 12 \text{ km s}^{-1}$ and $410 < V_a/\sqrt{K_0} < 530$ (where V_a is expressed in km s^{-1} and K in $\text{kpc}^2 \text{ Myr}^{-1}$). Furthermore, we show that the power law index for the diffusion coefficient is restricted to the interval $[0.45, 0.85]$, the best χ^2 being 25.5 for $\delta = 0.70$. For any δ in this interval, the good parameters in the $K_0/L - L$ and $V_a/\sqrt{K_0} - V_c$ planes can be straightforwardly deduced from the corresponding values for $\delta = 0.6$ by a simple scaling law. We exclude any model without a convective velocity or without reacceleration for any combination

of the three other diffusion parameters.

Our conclusions could get more stringent by new measurements in the whole energy spectrum for all nuclei. We emphasize that all our results were obtained using the best data, which are rather scarce and more than 20 year-old; new data are thus strongly needed. The AMS experiment on board the International Space Station will have in principle the ability to provide some of these data.

The next steps of this analysis will be to study radioactive species. In particular, we expect the recent SMILI data (giving the spectral distribution of Be isotopes over a large energy range) to provide a new insight on cosmic ray propagation, and thus to constraint further the diffusion parameters. We are also investigating the standard antiproton signal, using the results described in this paper.

Acknowledgments

We thank Aimé Soutoul for having pointed out a mistake in an early version of this paper. D.M. is particularly grateful for his remarks. F.D. gratefully acknowledges a fellowship by the Istituto Nazionale di Fisica Nucleare. We also would like to thank the French Programme National de Cosmologie for its financial support.

A. Solution for the diffusion model

Sources and interactions with matter are confined to the thin disk and diffusion which occurs throughout disc and halo with the same strength is independent of space coordinates. Sources follow a universal form $Q(E)q(r)$ with an associated normalization q_0^j for each nucleus (see § 3.5.2). Furthermore, we consider here only constant wind V_c in the z direction so that adiabatic losses (third term in (1)) vanish.

A.1. High energy limit

The dependence in energy E is implicit, and if we add radioactive contributions localized in both disc and halo

$$\left(\mathcal{L}_{diff} - \Gamma_{rad}^j \right) N^j(r, z) + \sum_{k=1}^{j-1} \Gamma_{rad}^{kj} N^k + 2h\delta(z) \left(q_0^j Q(E)q(r) + \sum_{k=1}^{j-1} \tilde{\Gamma}^{kj} N^k(r, 0) - \tilde{\Gamma}^j N^j(r, 0) \right) = \alpha \quad (\text{A1})$$

$$\mathcal{L}_{diff} = -V_c \frac{\partial}{\partial z} + K \left(\frac{\partial^2}{\partial z^2} + \frac{1}{r} \frac{\partial}{\partial r} \left(r \frac{\partial}{\partial r} \right) \right) \quad (\text{A2})$$

In our geometry a solution can be found in term of Bessel functions of zeroth order taking advantage of their properties (Jackson 1975). One can expand all the quantities over the orthogonal set of Bessel functions $\{J_0(\zeta_i x)\}^{i=1 \dots \infty}$,

$$N^j(r, z) = \sum_{i=1}^{\infty} N_i^j(z) J_0(\zeta_i \frac{r}{R}) \quad (\text{A3})$$

$$q(r) = \sum_{i=1}^{\infty} \hat{q}_i J_0(\zeta_i \frac{r}{R}), \quad \hat{q}_i = \frac{1}{\pi R^2 J_1^2(\zeta_i)} \frac{\int_0^1 \rho q(\rho) J_0(\zeta_i \rho) d\rho}{\int_0^1 \rho q(\rho) d\rho}, \quad \rho \equiv r/R \quad (\text{A4})$$

Such an expression respects automatically one of the boundary condition $N(r = R, z) = 0$. We will use a compact notation to describe the most general form for a source term

$$\bar{Q}^j = q_0^j Q(E) \hat{q}_i + \sum_k^{m_k > m_j} \tilde{\Gamma}^{kj} N_i^k(0) \quad (\text{A5})$$

Stable progenitors N^k As equations have to be valid order by order (second term of (A1) vanishes)

$$\left[\frac{d^2}{dz^2} - \frac{V_c}{K} \frac{d}{dz} - \left(\frac{\zeta_i^2}{R^2} + \frac{\Gamma_{rad}^{N^j}}{K} \right) \right] N_i^j(z) = \left(-\frac{\bar{Q}^j}{K} + \frac{2h\tilde{\Gamma}^j}{K} N_i^j(0) \right) \delta(z) \quad (\text{A6})$$

A fast procedure to solve (A6) is given by the following three steps:

1. Solution in the halo (no right-hand side in eq. (A6)) with the boundary condition $N_i^j(z = \pm L) = 0$

2. Integration ($\lim_{h \rightarrow 0} \int_{-h}^{+h} \dots dz$) of equation (A6) through the thin disc⁶, which gives

$$2N_i^j(z)|_{z=0} - 2N_i^j(0)\frac{V_c}{K} - 2hN_i^j(0)\frac{\tilde{\Gamma}^j}{K} + \bar{Q}^j = 0 \quad (\text{A7})$$

3. Put the halo solution in equation (A7) to ensure continuity between the two zones.

We finally obtain the solutions for stable progenitors in relativistic regime:

$$N^j(r, z) = \exp\left(\frac{V_c z}{2K}\right) \sum_{i=0}^{\infty} \frac{\bar{Q}^j}{A_i^j} \frac{\sinh\left[\frac{S_i^j(L-z)}{2}\right]}{\sinh\left[\frac{S_i^j L}{2}\right]} J_0\left(\zeta_i \frac{r}{R}\right) \quad (\text{A8})$$

$$\bar{Q}^j \equiv q_0^j Q(E) \hat{q}_i + \sum_k^{m_k > m_j} \tilde{\Gamma}^{kj} N_i^k(0) \quad (\text{A9})$$

$$S_i^j \equiv \left(\frac{V_c^2}{K^2} + 4\frac{\zeta_i^2}{R^2} + 4\frac{\Gamma_{rad}^{N^j}}{K}\right)^{1/2} \quad A_i^j \equiv 2h\tilde{\Gamma}_{N^j}^{tot} + V_c + K S_i^j \coth\left(\frac{S_i^j L}{2}\right) \quad (\text{A10})$$

For a primary $\bar{Q}^j = q_0^j Q(E) \hat{q}_i$, and for a pure secondary $\bar{Q}^j = \sum_k^{m_k > m_j} \tilde{\Gamma}^{kj} N_i^k(0)$. Note that solutions given in Webber et al. (1992) for secondary takes advantage of the primary form of $N_i^k(0)$. Since we are here interested in a *shower-like* (see § 3.2.2) resolution, the form given here is more adapted.

β decay contribution from N^k For all the nuclei treated here, N^j never has more than one unstable contribution, so that the sum over k for N_{rad}^k reduces to one term in equation (A1). Resolution is complicated by the localisation of this source in the whole halo. Focalsing on this specific term, neglecting for a while primary source and *classical* spallative secondary contribution $2h\delta(z) \sum_k \tilde{\Gamma}^{kj} N^k(r, 0)$, one obtains (following the same procedure as described in the previous section⁷)

$$N_{\Gamma_{rad}^k}^j(r, z) = \sum_{i=0}^{\infty} J_0\left(\zeta_i \frac{r}{R}\right) \times \frac{\Gamma_{rad}^{kj}}{K^j(a_i^2 - a^2)} \frac{N_i^k(0)}{\sinh\left(\frac{S_i^k L}{2}\right)} \quad (\text{A11})$$

⁶In terms of distribution (quoted in braces), defining σ_0 and σ_1 as the discontinuities of 0th et 1st order, remember that

$$\frac{\partial^2}{\partial z^2} \{\mathcal{F}(z)\} = \left\{ \frac{\partial^2 \mathcal{F}(z)}{\partial z^2} \right\} + \sigma_1 \delta(z) + \sigma_0 \frac{\partial \delta(z)}{\partial z}$$

Imposing the continuity of the vertical cosmic ray current across the plane $z = 0$, we thus have $\sigma_1 \equiv \lim_{\epsilon \rightarrow 0} [dN_i^j(z)/dz]_{-\epsilon}^{+\epsilon} = -2N_i^j(0)\frac{V_c}{K}$ and $\sigma_0 = 0$.

⁷The contribution of these radioactive nuclei may be unimportant in some cases, but we should take it into account as it is the dominant process for some others. In the simple example of $^{10}\text{Be} \rightarrow ^{10}\text{B}$, neglecting this channel would give an error of about 10% on the B flux, whereas considering that this term is only located in the disc would give an error of about 3% compared to the rigorous treatment given above. Notice finally that at fixed energy per nucleon, the rigidity depends on the nuclear species at stake. The diffusion coefficient K^j of the child nucleus j is therefore different from its progenitor's one K^k . The difference $K^j - K^k$ tends to vanish for the heaviest nuclei.

$$\times \left\{ \begin{array}{l} -\alpha a_i \cosh\left[\frac{S_i^j(L-z)}{2}\right] e^{\left(\frac{V_c z}{2K^j}\right)} + \left(a \sinh\left[\frac{S_i^k(L-z)}{2}\right] + a_i \cosh\left[\frac{S_i^k(L-z)}{2}\right] \right) e^{\left(\frac{V_c z}{2K^k}\right)} \\ + \frac{e^{\left(\frac{V_c z}{2K^j}\right)} \sinh\left[\frac{S_i^j(L-z)}{2}\right]}{A_i^j \sinh\left[\frac{S_i^j L}{2}\right]} \left[\begin{array}{l} \alpha a_i \cosh\left[\frac{S_i^j L}{2}\right] \left(V_c + 2h\tilde{\Gamma}^j + K^j S_i^j \tanh\left[\frac{S_i^j L}{2}\right] \right) \\ + \sinh\left[\frac{S_i^k L}{2}\right] \left[a \left(\frac{V_c K^j}{K^k} - 2V_c - 2h\tilde{\Gamma}^j \right) - a_i K^j S_i^k \right] \\ + \cosh\left[\frac{S_i^k L}{2}\right] \left[a_i \left(\frac{V_c K^j}{K^k} - 2V_c - 2h\tilde{\Gamma}^j \right) - a K^j S_i^k \right] \end{array} \right] \end{array} \right\}$$

where S_i^j and A_i^j have already been defined in (A10) and

$$\alpha \equiv \exp\left(\frac{V_c L}{2} \left(\frac{1}{K^k} - \frac{1}{K^j}\right)\right), \quad a \equiv \frac{V_c^2}{2K^k} \left(\frac{1}{K^k} - \frac{1}{K^j}\right) + \frac{\Gamma_{rad}^{kj}}{K^k} - \frac{\Gamma_{rad}^j}{K^j}, \quad a_i \equiv \frac{S_i^k V_c}{2} \left(\frac{1}{K^k} - \frac{1}{K^j}\right) \quad (\text{A12})$$

A.2. Full solution

Modifying relation (A1) so as to take into account energy losses and diffusive reacceleration is straightforward since those processes take place only in the disc and not in the halo. Following step by step the three point procedure previously described, one gets the differential equation⁸

$$A_i^j N_i^j(0) = \bar{Q}^j - 2h \frac{\partial}{\partial E} \left\{ b_{loss}^j(E) N_i^j(0) - K_{EE}^j(E) \frac{\partial}{\partial E} N_i^j(0) \right\} \quad (\text{A13})$$

where $b_{loss}^j(E)$ and K_{EE}^j respectively correspond to energy losses (described in section 3.6.1 and defined by (21)) and energy diffusion (reacceleration term given by (20)).

⁸For the β -unstable progenitor, the derivation is a bit more tedious but leads to the same final compact result.

REFERENCES

- Alves, D.R. 2000, *ApJ*, 539, 732
- Anders, E., & Grevesse, N. 1989, *Geochim. Cosmochim. Acta*, 53, 197
- Audi, G., Bersillon, O., Blachot, J., & Wapstra, A.H. 1997, *Nucl.Phys.A*, 624, 1
- Berezinskii, V.S., Buolanov, S.V., Dogiel, V.A., Ginzburg, V.L., & Ptuskin, V.S. 1990, *Astrophysics of Cosmic Rays* (Amsterdam: North-Holland)
- Binns W.R., & al. 1989, *ApJ*, 346, 997
- Blandford, R., & Eichler, D. 1987 *Phys.Rep.*, 154, 1
- Bloemen, J.B.G.M., Dogiel, V.A., Dorman, V.L., & Ptuskin, V.S. 1993, *A&A*, 267, 372
- Bondorf, J.P., Botvina, A.S., Iljinov, A.S., Mishustin, I.N., & Sneppen, K. 1995, *Phys.Rep.*, 257, 133
- Bradt, H.L., & Peters, B. 1950, *Phys.Rev.C*, 77, 54
- Case, G.L., & Bhattacharya, D. 1996, *A&AS*, 120, 437
———. 1998, *ApJ*, 504, 761
- Chen, C.X., & al. 1997, *Phys.Rev.C*, 56, 1536 and refs. therein
- Donato, F. & al. 2001, in preparation
- Donato, F. & al., 2001, in preparation
- Duvernois, M., & al. 1996, *A&A*, 316, 555
- Dwyer, R., & Meyer, P. 1987, *ApJ* 322, 98
- Engelmann, J.J., Goret, P., Juliusson, E., Koch-Miramond, Lund, N., Masse, P., Rasmussen, I.L., & Soutoul, A. 1985, *A&A*, 148, 12
- Engelmann, J.J., & al. 1990, *A&A*, 233, 96
- Fermi, E. 1949, *Phys.Rev.*, 75, 1169
———. 1954, *ApJ*, 119, 1
- Ferrando, P., Webber, W.R., Goret, P., Kish, J.C., Schrier, D.A., Soutoul, A., & Testard, O. 1988, *Phys.Rev.C*, 37, 1490
- Flesh, F., Heinrich, W., Röcher, H., Streibel, T., & Yasuda, H. 1999, *Proc. 26th Int. Cosmic-Ray Conf. (Salt Lake City)*, 1, 29
- Freedman, I., Giler, M., Kearsey, S., & Osborne, J.L. 1980, *A&A*, 82, 110
- García-Munoz, M., Simpson, J.A., Gusik, T.G., Wefel, J.P., & Margolis, S.H., 1987, *ApJS*, 64, 269

- Ginzburg, V.L., & Syrovatskii, S.I. 1964, *The origin of cosmic rays* (Pergamon Press)
- Ginzburg, V.L., Khazan, Ya.M., & Ptuskin, V.S. 1980, *Ap&SS*, 68, 295
- Grevesse, N., & Sauval, A.J. 1998, *Sp. Sci. Rev.*, 85, 161.
- Heinbach, U., & Simon, M. 1995, *ApJ*, 441, 209
- Ipavitch, F.M. 1975, *ApJ*, 196, 107
- Jackson, J.D., 1975 *Classical Electrodynamics* (John Wiley & sons)
- Jones, F.C. 1970, *Phys. Rev.*, 2, 2787
- Jones, F.C. 1979, *ApJ*, 229, 747
- Jones, F.C., Lukasiak, A., Ptuskin, V., & Webber, W., 2001, *ApJ*, in press (astro-ph/0007293)
- Ko, C.M., Dougherty, M.K., & McKenzie, J.F. 1991, *A&A*, 241, 62
- Korejwo, A., Giller, M., Dzikowski, T., Wdowczyk, J., Perelygin, V.V., & Zarubin, A.V. 1999, *Proc. 26th Int. Cosmic-Ray Conf. (Salt Lake City)*, 4, 267
- Kóta, J., & Owens, A.J. 1980, *ApJ*, 237, 814
- Krombel, K.E., & Wiedenbeck, M.E. 1988, *ApJ*, 328, 940.
- Kulsrud, R., & Pearce, W.P. 1969, *ApJ*, 156, 445
- Lerche, I., & Schlickeiser, R. 1982a, *A&A*, 107, 148
———. 1982b, *A&A*, 116, 10
———. 1985, *Proc. 19th Int. Cosmic-Ray Conf. (NASA. Goddard Space Flight Center)*, 3, 222
- Letaw, J.R., Silberberg, R., & Tsao, C.H. 1983, *ApJS*, 51, 271
———. 1984, *ApJS*, 56, 369
———. 1993, *ApJ*, 414, 601
- Lezniak, J.A., & Webber, W.R. 1979, *Ap&SS*, 63, 35
- Lukasiak, A., McDonald, F.B., & Webber, W.R. 1999, *Proc. 26th Int. Cosmic-Ray Conf. (Salt Lake City)*, 3, 41
- Mannheim, K., & Schlickeiser, R. 1994, *A&A*, 286, 983
- Norbury, J.W., & Townsend, L.W. 1993, *ApJS*, 86, 307
- Norbury, J.W., & Mueller, C.M. 1994, *ApJS*, 90, 115
- Nordgren, T.E. 1992, *AJ*, 104, 1465
- Ostrowski, M., & Siemienieć-Oziębło, G. 1997, *Astropart.Phys.*, 6, 271

- Owens, A.J. 1976, *Ap&SS*, 40, 357
- Parker, E.N. 1965, *ApJ*, 142, 584
———. 1966, *ApJ*, 145, 811
- Perko, J.S. 1987, *A&A*, 184, 119
- Prishchep, V.L., & Ptuskin, V.S. 1975, *Ap&SS*, 32, 265
- Ptuskin, V.S., Jones, F.C., & Ormes, J.F. 1996, *ApJ*, 465, 972
- Ptuskin, V.S., Voelk, H.J., Zirakashvili, V.N., & Breitschwerdt, D. 1997, *A&A*, 321, 434
- Ramsey, C.R., Townsend, L.W., Tripathi, R.K., & Cucinotta, A.F. 1998, *Phys.Rev.C*, 57, 982
- Reich, P., & Reich, W. 1988, *A&A*, 196, 211
- Schlickeiser, P., & Lerche, I. 1985, *Proc. 19th Int. Cosmic-Ray Conf. (NASA. Goddard Space Flight Center)*, 3, 54
- Schlickeiser, R. 1986, *Stochastic particle acceleration in CR (Shapiro)*
- Seo, E.S., & Ptuskin, V.S. 1994, *ApJ*, 431, 705
- Sihver, L., Tsao, C.H., Solberberg, R., Kanai, T., & Barghouty, A.F. 1993, *Phys.Rev.C*, 47, 1225
- Silberberg, R., & Tsao, C.H. 1990, *Phys.Rep.*, 191, 351
- Silberberg, R., Tsao, C.H., & Barghouty, A.F. 1998, *ApJ*, 501, 911
- Stanek, K.Z., & Garnavich, P.M. 1998, *ApJ*, 503, L131
- Stephens, S.A., & Streitmatter, R.E. 1998, *ApJ*, 505, 266
- Strong, A.W., & Moskalenko, I.V. 1998, *ApJ*, 509, 212
- Swordy, S.P., L’Heureux, J., Meyer, P., & Müller, D. 1993, *ApJ*, 403, 658
- Taddeucci, T.N., Ullmann, J., Rybarczyk, L.J., Butler, G.W., & Ward, T.E. 1997, *Phys.Rev.C*, 55, 1551
- Tripathi, R.K., Cucinotta, F.A., & Wilson, J.W. 1997a, *NASA Technical Paper*, 3621
———. 1997b, *NASA Technical Paper*, 3656
———. 1999, *NASA Technical Paper*, 209726
- Tsao, C.H., Silberberg, R., Barghouty, A.F., & Sihver, L. 1995, *ApJ*, 451, 275
- Tsao, C.H., Silberberg, R., & Barghouty, A.F. 1998, *ApJ*, 501, 920
- Tsao, C.H., & al. 1999, *Proc. 26th Int. Cosmic-Ray Conf. (Salt Lake City)*, 1, 13

- Vonach, H., Pavlik, A., Wallner, A., Drosch, M., Haight, R.C., Drake, D.M. & Chiba, S. 1997, Phys.Rev.C, 55, 2458
- Webber, W.R., Kish, J.C., & Schrier, D.A. 1990a, Phys.Rev.C, 41, 520
———. 1990b, Phys.Rev.C, 41, 533
———. 1990c, Phys.Rev.C, 41, 547
———. 1990d, Phys.Rev.C, 41, 566
- Webber, W.R., Lee, M.A., & Gupta, M. 1992, ApJ, 390, 96
- Webber, W.R. 1997, Space Sci. Rev., 81 107
- Webber, W.R., Soutoul, A., Kish, J.C., Rockstroh, J.M., Cassagnou, Y., Legrain, R., & 1998a, Phys.Rev.C, 58, 3539
- Webber, W.R., Kish, J.C., Rockstroh, J.M., Cassagnou, Y., Legrain, R., Soutoul, A., Testard, O., & Tull, C. 1998b, ApJ, 508, 940 and refs. therein
———. 1998c, ApJ, 508, 949 and refs. therein
- Wellish, H.P., & D.Axen, D. 1996, Phys.Rev.C, 54, 1329
- Werner, W. 1988, A&A, 201, 1
- Wiebel-Sooth, B., Biermann, P.L., Meyer, H. 1998, A&A, 330, 389
- Zeitlin, C., & al. 1997, Phys.Rev.C, 56, 388

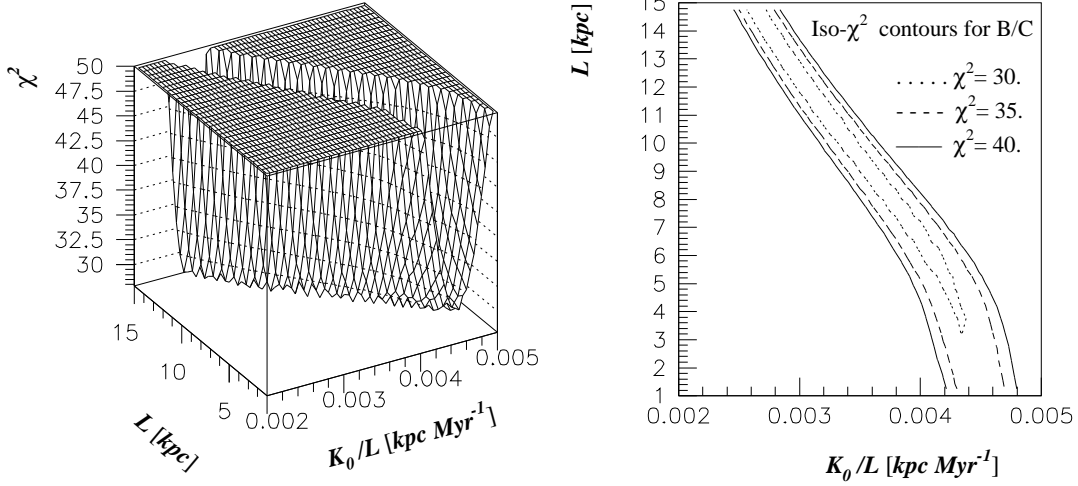


Fig. 1.— The χ^2 (adjustment to B/C data, see text) has been computed in all the parameter space for $\delta = 0.6$ (defined by $K = K_0 \mathcal{R}^\delta$). A best χ^2 is obtained for each L and K_0/L . Left figure displays the χ^2 values in the $K_0/L - L$ plane. It is truncated for $\chi^2 > 50$. Right figure shows the iso- χ^2 lines of the previous surface.

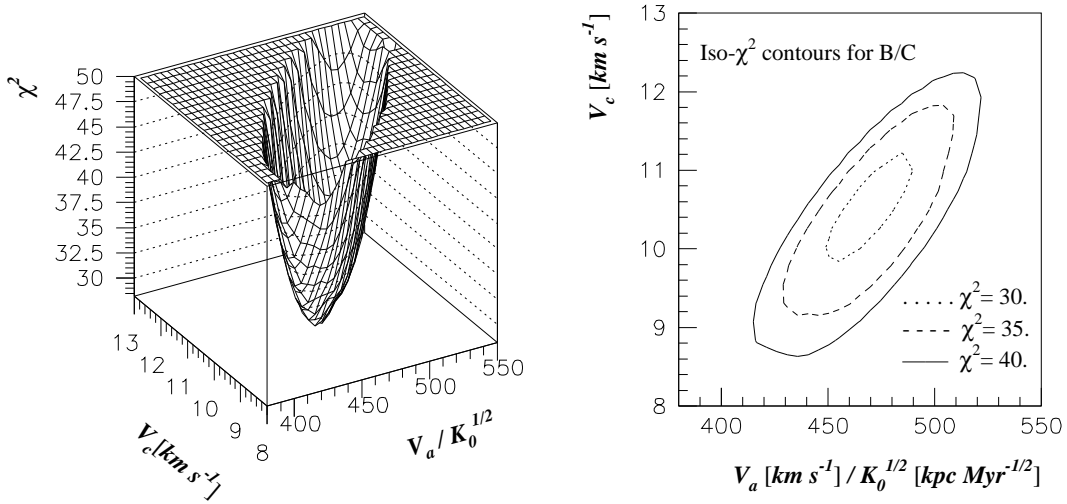


Fig. 2.— As in Fig. 1, a best χ^2 is obtained for each V_c and $V_a/\sqrt{K_0}$. Left and right figures are similar to those in Fig. 1.

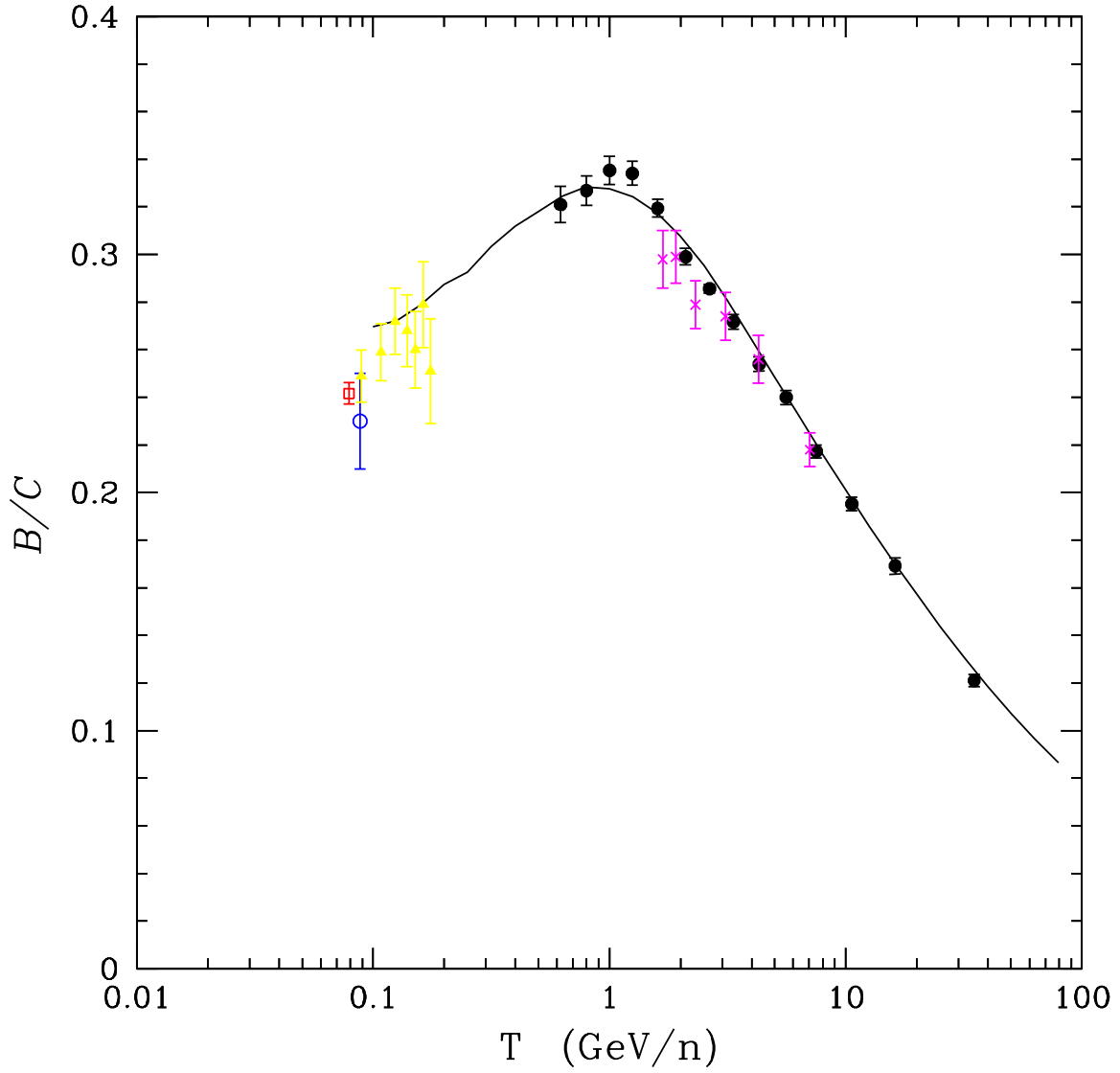


Fig. 3.— This curve displays the computed ratio of $(^{10}\text{B}+^{11}\text{B})/(^{12}\text{C}+^{13}\text{C}+^{14}\text{C})$ for a configuration giving a reduced $\chi_r^2 \approx 1.3$. The experimental points are from HEAO-3 (solid circles), ISEE (triangles), IMP-8 (empty circle), VOYAGER (square) and balloons (crosses).

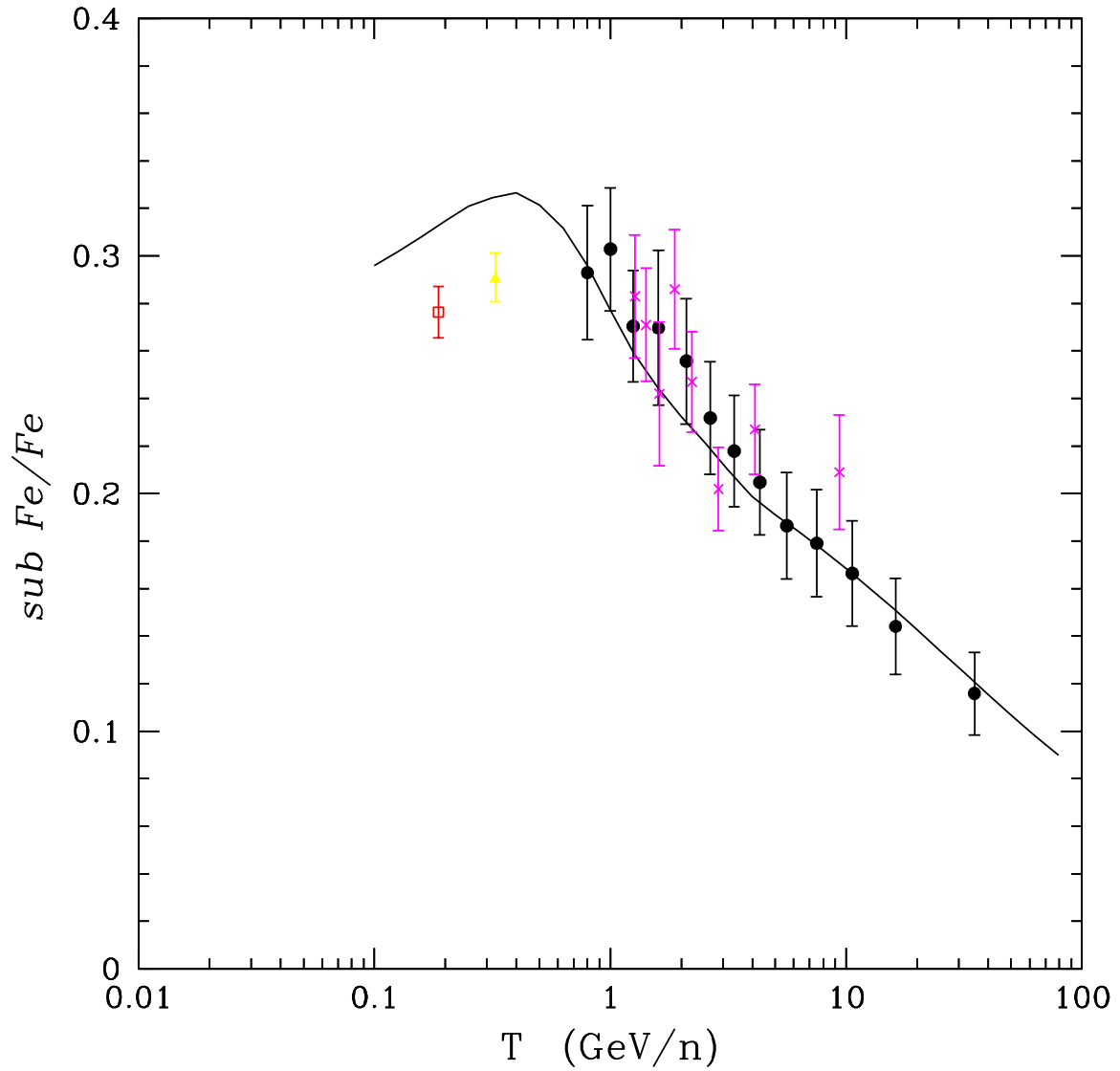


Fig. 4.— This curve displays the computed ratio of $(\text{Sc}+\text{Ti}+\text{V})/\text{Fe}$ for the same configuration as in Fig. 3. The experimental points are from HEAO-3 (solid circles), ISEE (triangles), VOYAGER (square) and balloons (crosses).

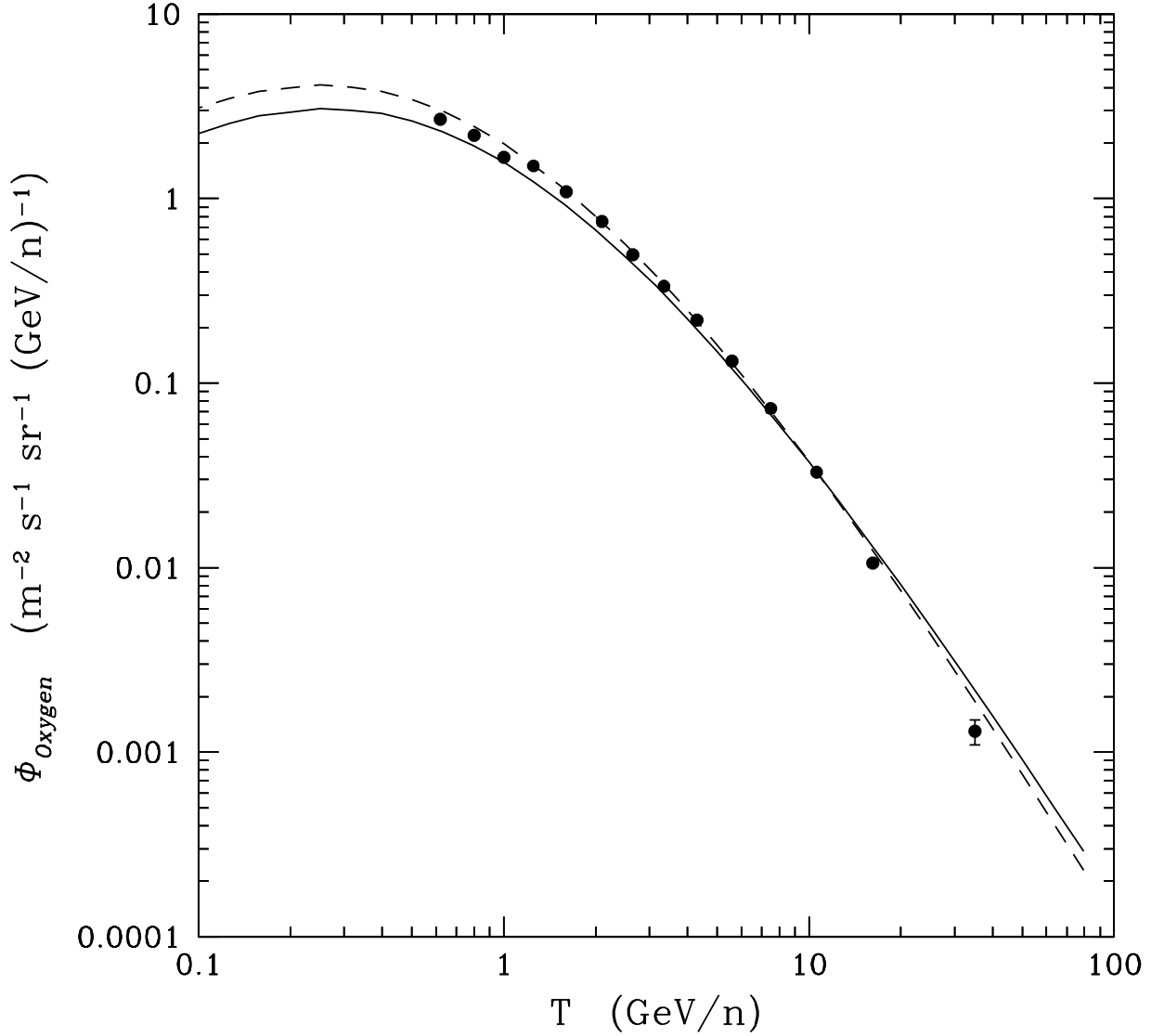


Fig. 5.— These curves display the computed flux of Oxygen for the same configuration as in figure 3. The solid line corresponds to $\delta + \alpha_{\text{Oxygen}} = 2.68$, the dotted line to $\delta + \alpha_{\text{Oxygen}} = 2.80$ (see text for details). The experimental points are from HEAO-3.

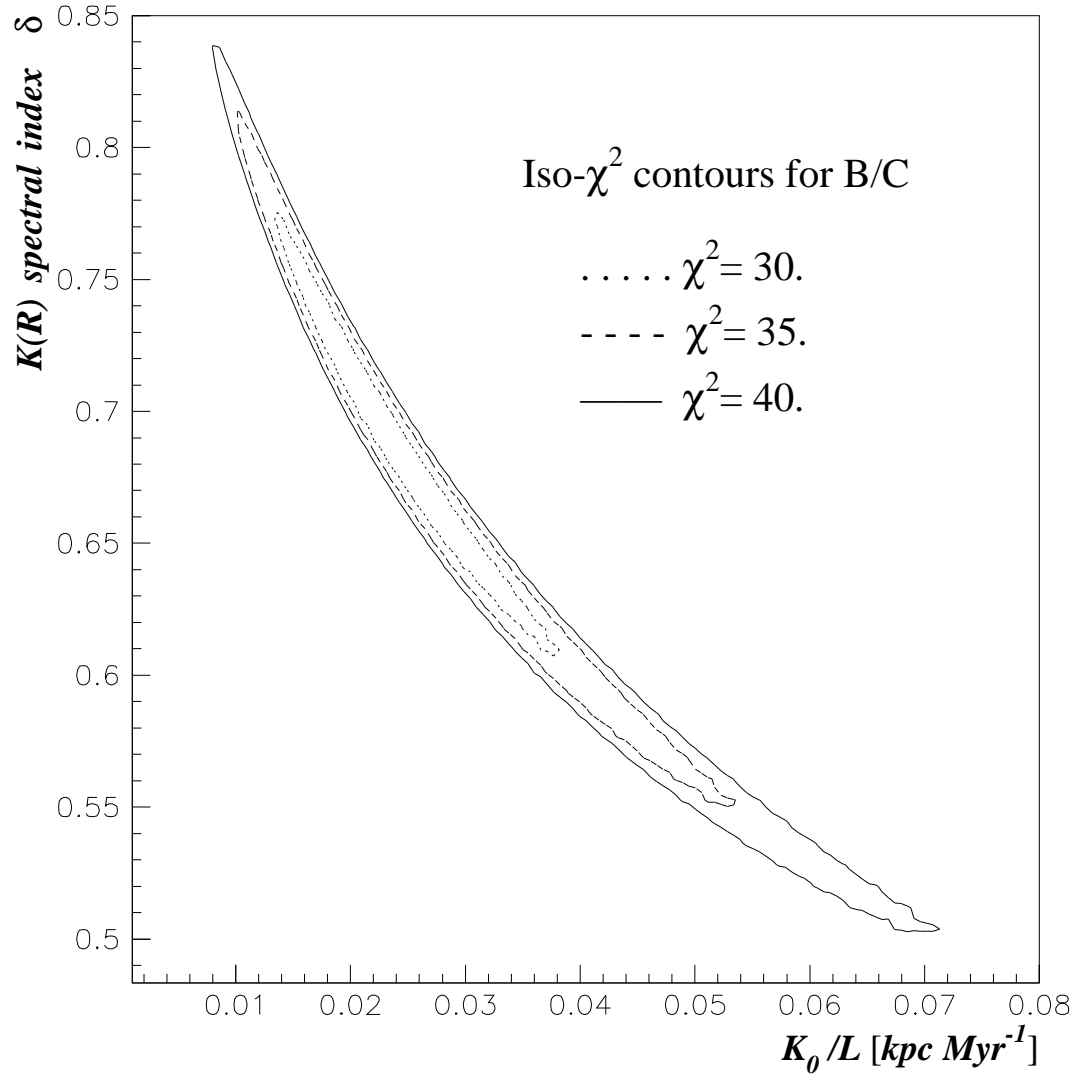


Fig. 6.— The parameter space has been explored for a fixed value of the halo thickness $L = 3$ kpc, varying δ (spectral index of K) as well as the other parameters. A best χ^2 is obtained for each δ and K_0/L . This figure shows the contour lines for fixed values of χ^2 .

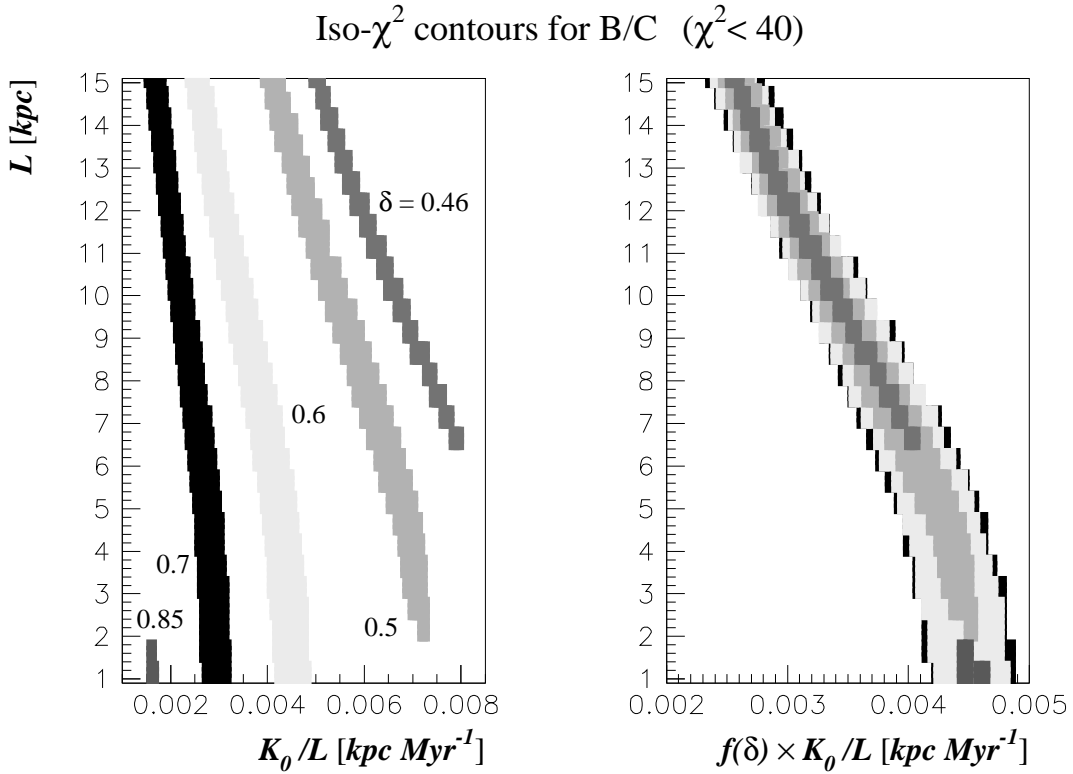


Fig. 7.— Models with different values of δ are shown. As in the previous figures, for each value of L and K_0/L , only the best χ^2 value is retained when the other parameters V_c and $V_a/\sqrt{K_0}$ are varied. The figure in the left panel displays the contour levels for $\chi^2 < 40$ for the indicated values of δ . It is possible to scale the K_0/L values by a function $f(\delta)$ to superimpose the contours corresponding to different values of δ (see text). This is displayed in the right panel.

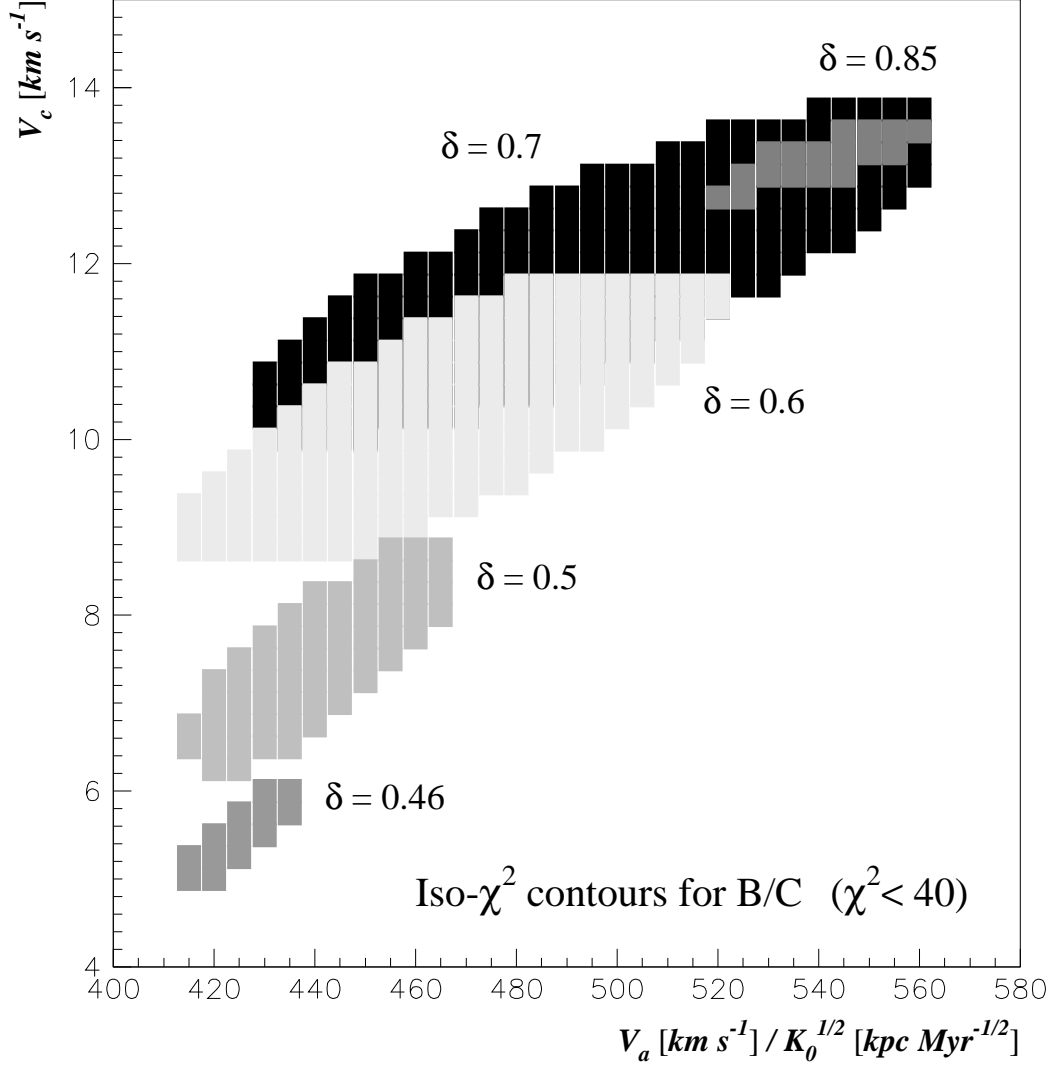


Fig. 8.— Models with different values of δ , the coefficient diffusion spectral index, are shown. For each value of V_c and $V_a/\sqrt{K_0}$, only the best χ^2 value is retained when the other parameters L and K_0/L are varied. The figure displays the contour levels for $\chi^2 < 40$ for the indicated values of δ .